Applied Thermal Engineering 205 (2022) 118053

Contents lists available at ScienceDirect

Applied Thermal Engineering

journal homepage: www.elsevier.com/locate/apthermeng

Comparative air conditioning performance using SiO_2 and Al_2O_3 nanolubricants operating with Hydrofluoroolefin-1234yf refrigerant

M.Z. Sharif [a,b], W.H. Azmi [a,b,*], N.N.M. Zawawi [b], M.F. Ghazali [b]

[a] Department of Mechanical Engineering, College of Engineering, Universiti Malaysia Pahang, Lebuhraya Tun Razak, 26300 Gambang, Kuantan, Pahang, Malaysia
[b] Centre for Research in Advanced Fluid and Processes, Lebuhraya Tun Razak, 26300 Gambang, Kuantan, Pahang, Malaysia

ARTICLE INFO

Keywords:
R1234yf
Nanolubricant
Cooling capacity
Compressor work
Coefficient of performance

ABSTRACT

Nowadays, the automotive air-conditioning system operating with Hydrofluoroolefin-1234yf or R1234yf refrigerant is used to reduce the global warming potential. This study aims to investigate the performance of SiO_2 and Al_2O_3 nanolubricants with R1234yf refrigerant in the automotive air conditioning system. The polyalkylene glycol-based nanolubricant was prepared using a two-step preparation method, and the stability of the nanolubricant was assessed using visual sedimentation observation and zeta potential analysis. The experimental investigation on the performance of automotive air conditioning system with R1234yf was undertaken for the SiO_2 and Al_2O_3 nanolubricants at different volume concentrations and various operating conditions. The system with SiO_2 nanolubricant at 0.01% volume concentration demonstrated the best cooling capacity performance with an average enhancement of 15.7%. On the other hand, the highest coefficient of performance increment and power consumption reduction were attained up to 9.8% and 27.1%, respectively for Al_2O_3 nanolubricant at 0.05% volume concentration. The SiO_2 nanolubricant performed with better cooling capacity, higher power consumption and lower coefficient of performance than the polyalkylene glycol-based lubricant. In contrast, the Al_2O_3 nanolubricant improved the coefficient of performance and reduced the power consumption. Since both nanolubricants provide their respective advantages, more research into integrating the two nanoparticles for refrigeration systems with R1234yf refrigerant is encouraged.

1. Introduction

Today, almost all vehicle manufacturers are focusing on producing vehicles with lower energy consumption. This is due to government policies that encourage vehicles to be more energy-efficient and produce fewer harmful gas emissions. The introduction of hybrid and fully electric vehicles powered by electric motors and internal combustion has encouraged further improvement to the automotive air conditioning (AAC) system. The current trend is focused on producing the AAC system with less impact on the environment and more energy efficiency. The AAC system is a parasitic load that draws some power from the engine. Nam [1] found that the use of AAC in a vehicle decreased the mileage by 20%, and increased the nitrogen oxides (NOx) by up to 80%. Currently, the world's use of AAC is increasing due to the increase in vehicles. The increment in global ambient temperature was contributed by many factors [2]. However, the main issue is the use of refrigerants with high global warming potential (GWP). The refrigerant will exit the AAC system in the event of a leak and an uncontrolled discharge. The refrigerant is released into the air and trapped in the atmospheric layer, simultaneously forming a layer that traps heat and reflects it back to the earth's surface. This condition is referred to as the greenhouse effect. Therefore, the primary concern of the present study is to focus on the replacement of the existing high GWP R134a refrigerant in the AAC system.

R1234yf is one of the alternative refrigerants to replace the existing refrigerant R134a. The R1234yf has a low GWP of four and zero ozone depletion potential (ODP) [3]. The molecular feature of R1234yf is that it is chlorine-free and has a short atmospheric life [4,5]. Moreover, the thermodynamic properties of R1234yf are almost similar to those of R134a. Thus, it can be directly used in the existing AAC system without any major modification to the original system. This refrigerant also complies with the European environmental regulations [6]. However, the AAC system with R1234yf (AAC-R1234yf) performs with a lower coefficient of performance (COP) than the existing refrigerant of R134a. Hence, many car makers still do not use R1234yf in their AAC systems,

* Corresponding author at: Department of Mechanical Engineering, College of Engineering, Universiti Malaysia Pahang, Lebuhraya Tun Razak, 26300 Gambang, Kuantan, Pahang, Malaysia.
E-mail addresses: wanazmi2010@gmail.com (W.H. Azmi), fairusham@ump.edu.my (M.F. Ghazali).

https://doi.org/10.1016/j.applthermaleng.2022.118053
Received 2 October 2021; Received in revised form 30 December 2021; Accepted 5 January 2022
Available online 10 January 2022

Nomenclature

Abbreviations

AAC	Automotive air conditioning
ASHRAE	American society of heating, refrigerating and air-conditioning engineers.
COP	Coefficient of performance
HFC	Hydrofluorocarbon
ODP	Ozone depletion potential
PAG	Polyalkylene glycol
RH	Relative humidity
rpm	Revolution per Minute
RSE	Relative standard error (%)
SAE	Society of Automotive Engineers
TXV	Thermostatic expansion valve
TEM	Transmission electron microscopy
VCRS	Vapour compression refrigeration cycle

Symbols

c_p	Specific heat for water at 303 to 313 K
m	Mass (kg)
$\dot{m}_w$	Water mass flow rate
$\dot{m}_r$	Refrigerant mass flow rate
m_{rc}	Initial refrigerant charge (g)
q_L	Heat Absorb (kJ · kg^{-1})
$\dot{q}_L$	Cooling capacity (kW) at refrigerant side
$\dot{q}_w$	Cooling capacity of (kW) from the calorimetric bath calculation
S_{err}	Standard error
T	Temperature (°C)
T_{in}	Average temperature for water inlet
T_{out}	Average temperature for water outlet
w_{in}	Compressor work (kJ · kg^{-1})
$\dot{w}_{in}$	Compressor power (kW)

Greek Symbols

ϕ	Volume concentration (%)
ρ	Density (kg · m^{-3})
σ	Standard deviation for sample

Subscripts

L	Lubricant
P	Nanoparticle

as pointed out by a few recent studies [5,7,8]. Today, various technologies and strategies are being used to improve the vapour compression refrigeration systems (VCRS) and the AAC systems. Some of the options to improve the energy efficiency of the air conditioning system are suggested, such as upgrading the system components, improving the operational management, and revising the control strategies [9]. Currently, most AAC systems with R1234yf are focused on improving the components of the system. Additional components such as internal heat exchangers (IHX) and ejectors are used in the AAC system to improve the efficiency. However, the modification of the AAC component requires significant changes to the overall system, making it complicated. In addition, the development of the new component is time-consuming and requires extra maintenance costs due to the installation of additional components. Therefore, another option for improving the AAC system is to use recent nanotechnology to improve the properties of AAC working fluids such as refrigerants and lubricants [10].

Nanoparticles are dispersed into the existing lubricants to enhance the thermo-physical properties and are known as nanolubricants. Enhancement of the thermo-physical properties of nanolubricants such as thermal conductivity and viscosity has been reported in several recent studies [11,12]. The alteration of thermo-physical properties is one of the key solutions to enhance the VCRS performance for flow boiling heat transfer in the evaporator and condensation heat transfer in the condenser [4,13]. The nanolubricants also performed better than the original lubricants for tribology properties as well as rheology properties. Some of the improvements to tribology properties, for instance, coefficient of friction (COF), wear rate, and tear, have been reported in the recent literatures [14,15]. A small addition of nanoparticles into lubricants will slightly increase the viscosity of nanolubricants. A thicker viscosity of lubricant can maintain a better oil film between the moving surfaces, thus reducing friction. Although the viscosity of the lubricant is essential in mechanical systems, high viscosity will increase the power consumption. Thus, an optimum concentration of nanolubricants is necessary. Due to the increase in heat transfer capability and tribology performance, the recent study was reported with significant enhancement of VCRS efficiency with nanolubricants [10].

However, to date, the effectiveness of nanolubricants in the VCRS using R1234yf is not available in the literature. Despite all the advantages of nanolubricants, no related studies have been done with nanolubricants in the AAC-R1234yf system. Thus, an experimental evaluation is required to study the performance of the AAC-R1234yf system with nanolubricants. The use of nanolubricants with R1234yf in the AAC system is expected to solve the issues of performance, energy consumption, and the environment. Therefore, a systematic experimental performance investigation at different volume concentrations as well as different types of materials for SiO_2 and Al_2O_3 nanolubricants is performed in this paper to evaluate the applicability of the new type of polyalkylene glycol (PAG ND12) nanolubricants with R1234yf in the AAC-R1234yf system.

2. Methodology

2.1. Test rig and experimental setup

The test rig was developed for air conditioning system with a cabin capacity of 2370.82 L and was initially designed for a compact car. The test rig includes a Sanden compressor (SWJ-7B08) with a multichannel condenser and evaporator with a static bulb thermostatic expansion valve (built to operate with 115 to 130 g optimal charge for the R134a and R1234yf refrigerants). The test rig is fully equipped with nine thermocouples, pressure gauges, and power meter to monitor the temperatures, inlet and outlet pressures, as well as compressor energy usage throughout the experimental test. Fig. 1(a) and 1(b) show the schematic diagram and experimental test rig, respectively. Table 1 summaries the materials and equipment for the experiment. Table 2 shows the test rig instrumentation ranges and uncertainty.

The AAC system in the present experiment was designed with capability to maintain the refrigerant temperature at 28 °C ± 1 °C before entering the compressor, regardless of the amount of refrigerant charge and compressor speed. The thermostatic expansion valve (TXV) will control the refrigerant mass flow rate and system pressure to maintain the temperature at this condition. In addition, the surrounding environment near the AAC test setup was controlled and maintained at the temperature of 25 °C ± 0.5 °C and the humidity of 60 RH ± 10 RH [16]. The surrounding temperature and humidity were controlled to ensure the experimental data was under the same environmental conditions. The isentropic efficiency for the present AAC system is found between 80% and 100% with an average of 88% at all ranges of initial refrigerant charge and compressor speed.

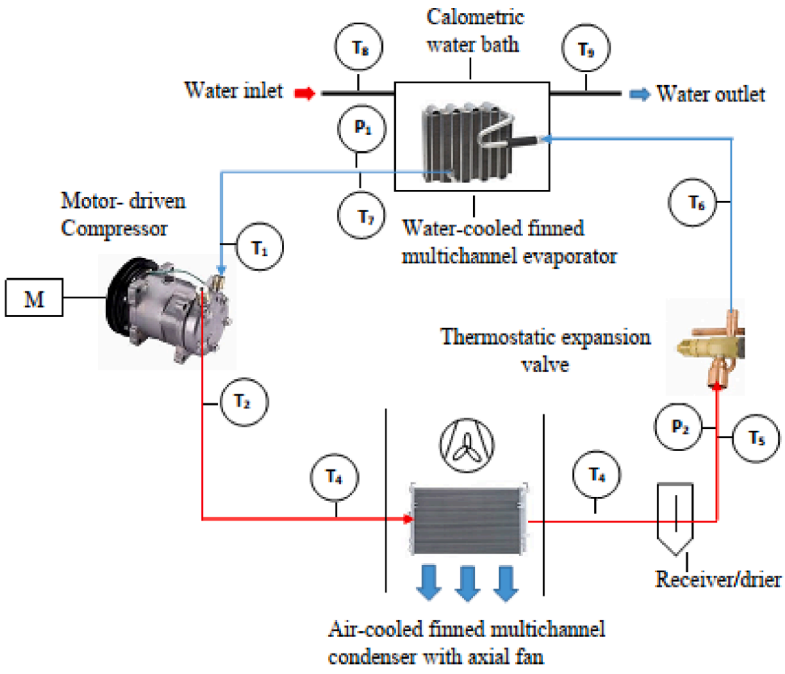

a) Schematic diagram of AAC

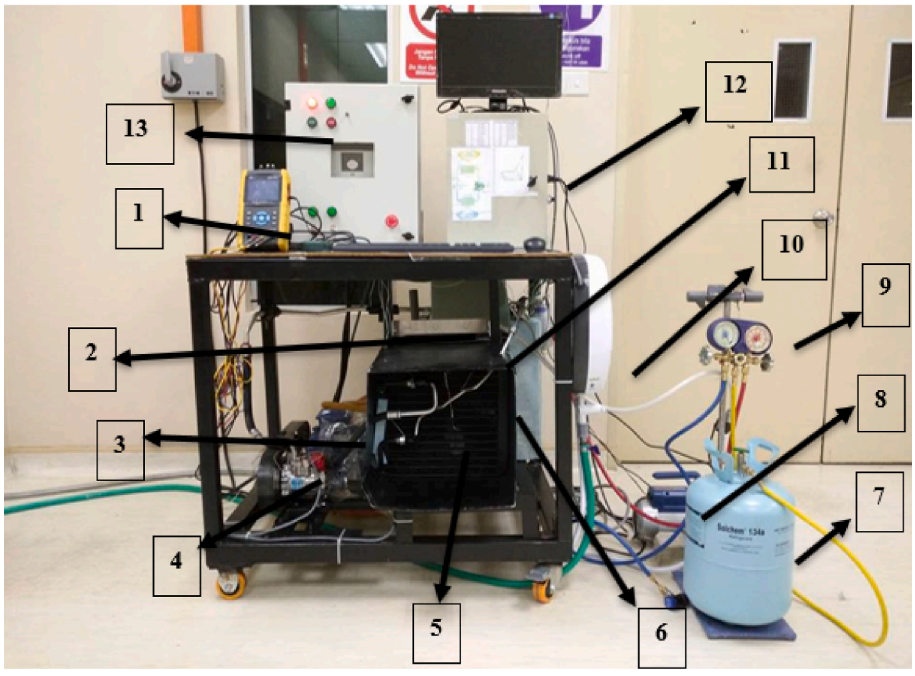

b) Experimental setup with data logging system

Fig. 1. The schematic diagram for experimental setup of the AAC system.

Experiments were conducted to investigate the performance of the test rig to determine: (i) the effect of initial refrigerant charge (90 to 120 g) on AAC performance; (ii) the effect of compressor speed (900 to 2100 rpm) on AAC performance; and (iii) the comparison of AAC performance with different types of lubricants, namely PAG lubricant, SiO_2/PAG, and Al_2O_3/PAG nanolubricants at different volume concentrations. The SiO_2 nanoparticles was manufactured by Beijing DK Nanotechnology and the Al_2O_3 nanoparticles was procured from Sigma-Aldrich. The SiO_2 and Al_2O_3 nanoparticles were obtained with average particle sizes of 30 and 13 nm, respectively, with 99.9% purity. In the present study, the nanoparticles was kept in a dry cabinet under controlled temperature and humidity to avoid any excessive moisture. Therefore, no heat treatment is required to dry the nanoparticles. The characteristics of nanoparticles are presented in Table 3. On the other hand, the characteristics of R1234yf refrigerant [17] and PAG ND12 lubricants [18,19] are shown in Table 4.

Table 1
- Summary of materials and equipment for the experiment.

Notation	Materials/ Equipment	Description
1	Power Analyser	3-phase Power analysers from Lutron (model DW-6092) were used to measure electrical power characteristics and power consumption of the induction motor used to drive the compressor.
2	Evaporator	An evaporator is a heat exchanger with the function to absorb heat from the refrigerated space
3	Electric Motor	A 2.2 kW and 3-phase induction motor that drives the compressor via a belting system. The maximum speed of the motor is 2850 rpm.
4	Compressor Type J8302	The rotary vane fixed displacement compressor is commonly used in compact car type AAC system. The compressor has a maximum of 1.2 kW refrigeration capacity.
5	Condenser	The condenser is a heat exchanger with the function to release heat from the hot gas refrigerant discharged from the compressor to liquid-state refrigerant.
6	Fan behind the condenser	The fan forces the airflow to pass through the condenser to remove the heat from the condenser.
7	Refrigerant, R1234yf	Refrigerant is a working fluid of the refrigeration system by utilising the phase changes from liquid to gas and back again to cool down the temperature of cars and buildings.
8	Air vacuum device	A device to remove air and moisture from the setup by sucking them and creating vacuum pressure. The device is also used to check leakage of refrigerants.
9	Pressure gauge	An instrument to read the pressure reading in the high side and low side of the system.
10	Water heater	A 3.6 kW water heater to heat up the inlet water of the evaporator calorimetric system. It is also integrated with the pump and flow meter to maintain the constant flow rate of water and take the water flow reading.
11	Water tank	An insulated 60-litre water tank for the purpose of the evaporator calorimetric system. The evaporator will be placed inside of the tank; thus, the cooling capacity and the mass flow rate of the system will be determined.
12	Computing system device	It consists of a PC integrated with 16 channels data loggers of the temperature measurements. All the readings were stored in a computer.
13	Frequency Inverter	A 4-kW capacity frequency inverter was employed to run the electrical motor and control the compressor revolution speed.

Table 2
Test rig instrumentation ranges and uncertainty.

No	Measured Data	Model	Range	Uncertainty
1	Pressure	Testo 550 digital pressure gauge	0 – 6.5 MPa	± 0.001 MPa
2	Temperature	RS PRO Type K Thermocouple 0.6 mm Diameter	− 50 °C to 250 °C	± 0.1 °C
3	Power consumption	Lutron DW-6092 Digital watt/ Power Meter	0 – 9.99 kW	± (1%+ 0.008 kW)

2.2. Preparation of nanolubricants and experimental procedure

A two-step preparation was used to produce various PAG lubricant mixtures using SiO_2 and Al_2O_3 nanoparticles as additives at 0.01, 0.03, and 0.05% volume concentrations. The two-step approach was widely employed in the literature and was discovered to be the most reliable method in the preparation of nanolubricants [20–22]. The present study was considered the nanolubricants at volume concentration of 0.01 to 0.05% and was recommended in the prior studies [23,24]. Redhwan et al. [23] and Sharif et al. [24] proposed an optimum volume concentration of 0.01% and 0.05% for Al_2O_3/PAG and SiO_2/PAG nanolubricants, respectively, for the base lubricant PAG ND8 in the AAC system. Therefore, in the present study, the volume concentration of nanolubricants is considered to be between 0.01% and 0.05%. The quantity of nanoparticles was measured using a digital measurement scale and calculated by considering the volume of compressor lubricants using **Eq. (1)**. An ultrasonic bath vibrator was used to disperse the nanoparticles in the mixture for up to 2 h, resulting in a homogeneous PAG-based nanolubricant at different volume concentrations.

$$\varphi = \left(\frac{m_p}{\frac{m_p}{\rho_p} + V_{PAG}} \right) \times 100\% \quad (1)$$

In this experiment, the ultrasonic bath was manufactured by Fisherbrand Scientific with a model number of FB15051. The ultrasonic bath was designed with 80 W of ultrasonic mean power and the constant frequency of 37 kHz. The sonication parameter was fixed for this model and was used in the preparation of the present nanolubricants. Two hours of sonication time is considered in the preparation of nanolubricants to avoid any excessive overheating throughout the sonication process. The temperature and volume of water are kept constant and changed every half hour to maintain a consistent temperature. The ultrasonic bath was recommended for stability improvement of nanolubricant in the previous study [25]. The visual sedimentation observation method and zeta potential analysis were used to assess the stability condition of the present nanolubricants.

Nanolubricants is a combination of PAG lubricants and nanoparticles with a size of less than 100 nm. In the present study, the characterization of the nanoparticles in liquid suspension was done by using transmission electron microscopy (TEM). TEM was useful to investigate the

Table 3
Properties of Al_2O_3 and SiO_2 nanoparticles at room temperature [45,46].

Property	Al_2O_3	SiO_2
Average Particle diameter, nm	13	30
Thermal Conductivity, W/m · K	36	1.4
Purity, %	99.9	99.9
Specific heat, J/kg · K	773	745
Molecular mass, g/mol	101.96	60.08
Density, kg/m^3	4000	2220
CAS number	a. 1344–28-1	14808–60-7

Table 4
The characteristic of refrigerant R1234yf [17] and PAG ND12 lubricants [18,19].

	R1234yf	PAG ND12
Chemical formula	2,3,3,3 - tetrafluoropropene	
Chemical name	$CF_3CF = CH_2$	
Group of refrigerants	Hydrofluoroolefin (HFO)	
ASHRAE safety classification	A2L – non-toxic & mildly-flammable	
Critical pressure (bar)	34	
Critical temperature (°C)	95	
Boiling point @ 1 atm (°C)	−29	
ODP	0	
GWP	1	
ISO viscosity grade		46 cP
Density		1.021 g.cm^{-3} (40 °C) 0.976 g.cm^{-3} (100 °C)
Viscosity index		216.157
Kinematic viscosity		39.3 mPa.s (40 °C) 8.45 mPa.s (100 °C)
Flash point		−36 °C

agglomeration and characterization of the nanoparticles in their suspended form. It is crucial to review the size, shape, and dispersion form of nanolubricants, especially for the application of nanolubricants in the actual environment of the AAC system. This is because these parameters will affect the stability of actual dispersion in the system [26] and will alter the thermo-physical properties of the nanolubricant [27]. Therefore, the TEM was used to detect nanoparticles dispersion in PAG lubricants at high magnification scales. Subsequently, TEM scanning was used to estimate the average size, shape, and condition of the suspended nanoparticles in the nanolubricants solution. The cross-section region of each nanoparticle shown in the TEM image was determined to approximate the average size of the particle diameter. The TEM images of nanolubricants with nanoparticles (Al_2O_3 and SiO_2) are shown in Fig. 2. From the TEM images, the Al_2O_3 and SiO_2 nanoparticles shapes are observed to be spherical. Fig. 2(a) shows the image of Al_2O_3 nanoparticles in lubricants with a magnification of × 88,000 and a scale of 50 nm. The figure confirmed the spherical shape and 13 nm size of Al_2O_3 nanoparticles, hence in agreement with the data provided by the manufacturer. Besides, Fig. 2(a) also shows the good dispersion condition of Al_2O_3 nanoparticles in PAG lubricants at this magnification scale. Fig. 2(b) presents the TEM image of SiO_2/PAG nanolubricants at a magnification of × 88,000 with a scale of 50 nm. SiO_2 nanoparticles were observed in a spherical shape and complied with the data stated by the manufacturer. The SiO_2 nanoparticles dispersion state in PAG lubricants was also found in good condition with minimal agglomeration. The distribution of the particle size was observed to be within ± 30 nm. The average size and shape of the individual Al_2O_3 and SiO_2 nanoparticles distribution in PAG lubricants were confirmed in Fig. 2(a) and 2(b), respectively.

For each experiment, homogeneous mixtures of nanolubricant at various volume concentrations were injected into the compressor. The test rig was flushed with a vacuum pump in preparation for another experimental trial. The vacuum process is used to remove all refrigerants, compressor lubricants, and any moisture in the system. The experimental procedure for the AAC performance investigation followed the regulations and recommendations of the SAEJ2765 standard [16]. This method allowed the AAC system to start 20 min earlier, allowing the system to reach steady state. After 20 min, the pressure and temperature of the AAC system were recorded for 10 min and continued with experimental data analysis.

2.3. Experimental analysis

The measured data such as pressure, temperature, and compressive power consumption were used to calculate some crucial parameters, including saturated vapour enthalpy at the compressor inlet (h_1), hot vapour enthalpy at the compressor outlet (h_2), and vapour enthalpy at the evaporator inlet (h_6). The typical *P-h* diagram of the present VCRS cycle is shown in Fig. 3. All the calculations in the manuscript are based

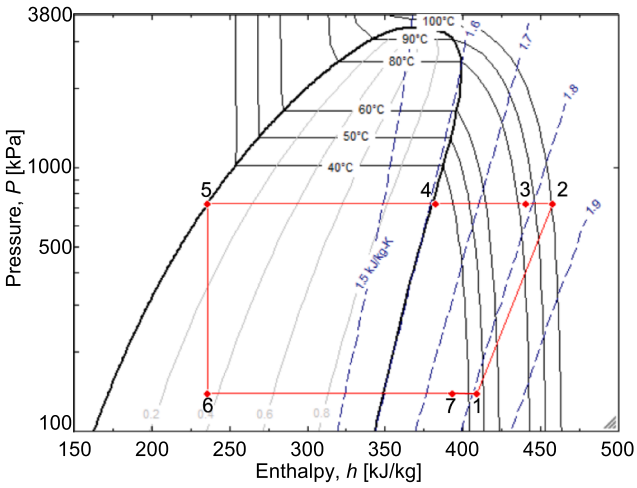

Fig. 3. *P-h* diagram of present VCRS cycle for R1234f refrigerant.

on the assumption of the ideal condition for the experimental analysis. Engineering Equation Solver (EES) software was used to calculate these data. All experimental data were analyzed to determine the behaviour of cooling heat transfer on the platform and to calculate COP, heat absorb (q_L), cooling capacity ($\dot{q}_L$), compressor work (w_{in}), compressor power ($\dot{w}_{in}$), subcooling (t_{sc}) and superheating (t_{sh}). The ability of the evaporator to absorb heat and the cooling capacity are used to evaluate the cooling effect of the AAC system. **Eq. (2)** describes the heat absorb calculation for the evaporator. The wind tunnel is replaced by a waterway in the evaporator area where the evaporator is immersed in a well-insulated container. The inlet temperature of the water passing through the evaporator is kept constant at 30 °C ± 0.5 °C. The difference between the inlet and outlet temperatures is used to calculate the cooling capacity by assuming the cooling effect of the evaporator is similar to the heat absorbed from the water. **Eq. (3)** defines the equation for cooling capacity [28].

$$q_L = h_6 - h_1 \tag{2}$$

$$\dot{q}_L = \dot{q}_w = \dot{m}_w c_p \left(T_{w,out} - T_{w,in}\right) \tag{3}$$

The variation of the mass flow rate ($\dot{m}_r$) for all experimental trials was calculated by following ASHRAE Standard 41.1–1986 [28]. This is done by finding the ratio of the measured cooling capacity utilisation and the heat absorb input at the steady-state, thus giving the mass flow rate for each experiment. **Eq. (4)** represents the refrigerant mass flow rate equation.

$$\dot{m}_r = \frac{\dot{q}_L}{q_L} \tag{4}$$

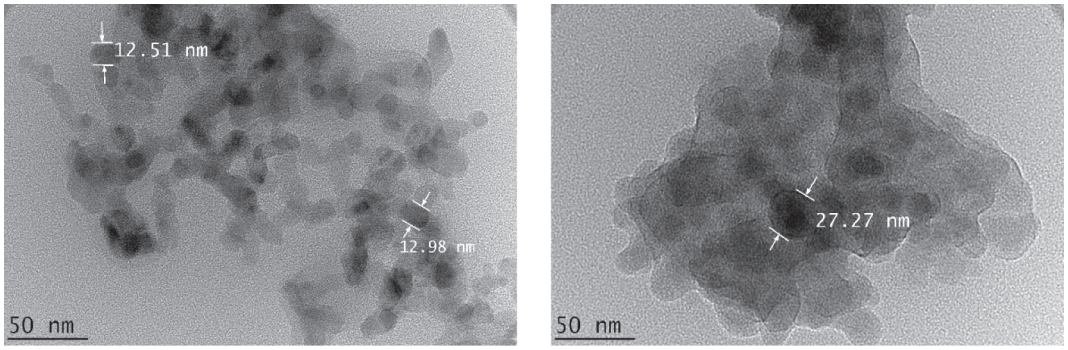

a) Al_2O_3/PAG nanolubricants b) SiO_2/PAG nanolubricants

Fig. 2. TEM images of nanolubricants at X 88,000 magnifications.

The impact on the compressor in the AAC system is evaluated based on the power consumption and the input or output compressor. **Eq. (5)** describes the compressor work calculation for the AAC system.

$$w_{in} = h_2 - h_1 \tag{5}$$

Eq. (6) represents the compressor power calculation, and **Eq. (7)** defines the COP equation.

$$\dot{w}_{in} = \dot{m}_r(h_2 - h_1) \tag{6}$$

$$\text{COP} = \frac{q_L}{w_{in}} \tag{7}$$

In addition, the following assumptions are considered during the experimental investigation: (i) The discharge and condensation pressure deviations can be ignored, (ii) the evaporator inlet and outlet deviations can be ignored, (iii) the enthalpies at the condenser and evaporator exits are assumed to be the same ($h_5 = h_6$), and (iv) the cooling effect on the system can be ignored.

2.4. Consistency analysis

The data collection measurement errors for all performance parameters were calculated based on the percent relative standard error (RSE) presented by Yusri et al. [29]. According to Yusri et al. [29], consistency analysis is performed to ensure the reliability and reproducibility of the experimental results. As shown in **Eq. (8)**, the relative standard error (RSE) method is used to determine the consistency and precision of the experimental data. The mean of the sample collection is denoted by X , the standard deviation is denoted by σ, and n represents the number of samples. Each experiment is repeated three times to acquire the average percentage of RSE. Table 5 illustrates the parameters of consistency. The maximum RSE is reported to be less than 1.22% for all parameters and within an acceptable range.

$$RSE = \frac{S_{eer}}{X} \times 100 \text{ where the Standard error } S_{eer} \text{ is calculated using } S_{eer} = \frac{\sigma}{\sqrt{n}} \tag{8}$$

3. Results and discussion

3.1. Stability of nanolubricant

Researchers have described stability as nanolubricants validity [30]. The stability of nanolubricants is essential for the final application in commercial vehicles. Usually, most of the time, the vehicle is stored in a parking lot. In a continually moving system, nanolubricants will not experience any problems. This is because the vibration and compression processes experienced in the air-conditioning system will prevent the nanoparticles in the lubricants from clumping and settling. Instead, the nanolubricants in a stationary condition for a long time will cause them to clump and, subsequently, sediment in the air-conditioning system. Therefore, most of the stability studies for nanolubricants have been carried out in a stationary state. The nanolubricants with excellent stability and good nanoparticles dispersion in the base lubricants will have better thermo-physical properties [31]. The stability of nanolubricants will be examined in terms of the tendency for agglomeration and long-term deposition rates. In this study, nanolubricants stability will be measured immediately after preparation. The stability of the nanolubricants was measured by qualitative (visual sedimentation observation) and quantitative (zeta potential analysis) approaches.

Table 5
Percentage of relative standard error for the experimental performance parameters.

Speed (rpm)	Percentage relative standard error, RSE (%)				
	q_L	Q_L	COP	$\dot{m}$	W_{in}
900	0.99	0.03	0.35	0.98	0.33
1200	0.52	0.03	0.13	0.53	0.11
1500	0.36	0.01	0.09	0.39	0.09
1800	1.22	0.04	0.25	1.17	0.21
2100	0.90	0.04	0.19	0.92	0.21

3.1.1. Visual sedimentation observation

The stability of SiO_2/PAG and Al_2O_3/PAG nanolubricants was observed using visual sedimentation analysis. The samples were presented in several identical test tubes. After the preparation process, the nanolubricants were aseptically transferred into the test tube. Then, visual observation was carried out by identifying the aggregation and deposition of the sample with time. Subsequently, the images of the samples were captured on the first day and after six months of preparation, as shown in Fig. 4. The figures indicate the stability conditions for various nanolubricants at different volume concentrations of 0.01% to 0.05%. All nanolubricants samples showed excellent stability conditions without a visible trace of particles settling down at the bottom of the test tube. As shown in Fig. 4(a), SiO_2/PAG nanolubricants had an excellent stability at all volume concentrations with no visible particle settling.

The opacity of the Al_2O_3/PAG nanolubricant in Fig. 4(b) on the other hand was gradually reduced at the top layer of the samples. However, these phenomena were not applicable to the SiO_2/PAG sample. The present outcome for static visual stability observation was confirmed as an excellent stability condition for present nanolubricants for a maximum period of 6 months. Hence, these results had supported the potential of nanolubricants for application in the AAC system. It was expected that the nanolubricant will not pose any significant problems related to stability. Interestingly, these findings show that the nanolubricant was stable for up to 6 months, which was longer than previous studies in the literature [32–35]. However, further investigation on stability by quantitative approaches needs to be conducted to verify the stability condition of the present nanolubricants. Therefore, the following section presents the results for stability evaluation using zeta potential under quantitative measurement.

3.1.2. Zeta potential analysis

Zeta potential is a scientific term for the electrokinetic potential in colloidal dispersions. The zeta potential study was performed after the nanolubricants preparation process. The purpose of this evaluation is to study the ability of nanoparticles to prevent agglomeration in the base fluids. The zeta potential test is a study to measure the strength of rejection among nanoparticles. Nanolubricants samples are considered stable and difficult to clamp if it have zeta potential of $\pm$ 30 mV or above [36]. The variation of zeta potential for SiO_2/PAG and Al_2O_3/PAG nanolubricants were shown in Fig. 5. The SiO_2/PAG and Al_2O_3/PAG nanolubricants were performed with a high zeta potential of 80.6 and 82.6, respectively. Based on previous studies, zeta potential values had several levels of stability, from low to high values [26,36]. The nanolubricants with zeta potential of more than 60 mV had shown excellent stability. Therefore, the zeta potential of the samples in the present study was found to be above 60 mV, confirming the nanolubricants' stability and applicability for application in the AAC system. The nanolubricants samples with high zeta potential tended to have less accumulation and deposition. This was due to the higher repulsion force between the nanoparticles inside the supernatant fluids. The zeta potential of the Al_2O_3/PAG nanolubricant with PAG ND12 in the present study showed significant improvement compared to the work by Redhwan et al. [23] and Zawawi et al. [35] for Al2O3/PAG and Al2O3-SiO_2/PAG nanolubricants, respectively, with PAG ND8.

3.2. Refrigerant mass flow Rate, superheating and subcooling

Before delving deeper into the critical parameters of the AAC-R1234yf system, it is essential to analyse some additional or support

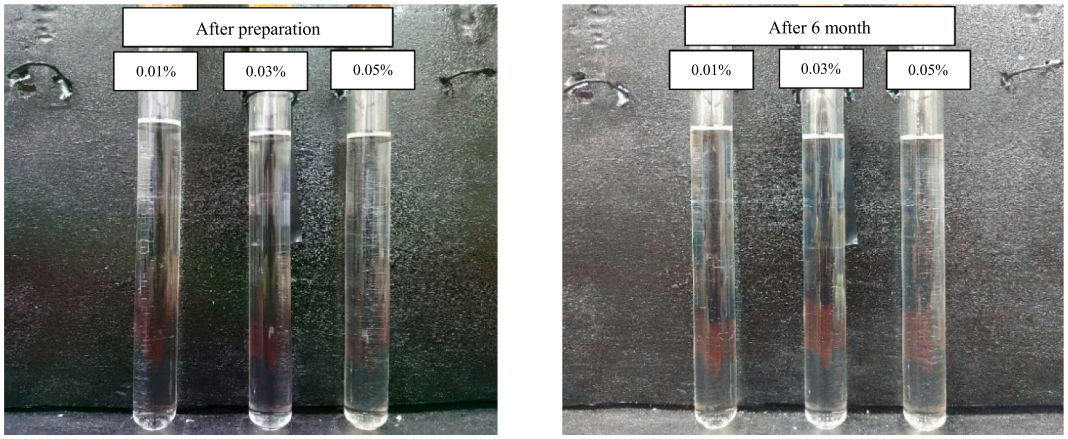

(a) Visual sedimentation for SiO_2/PAG nanolubricants

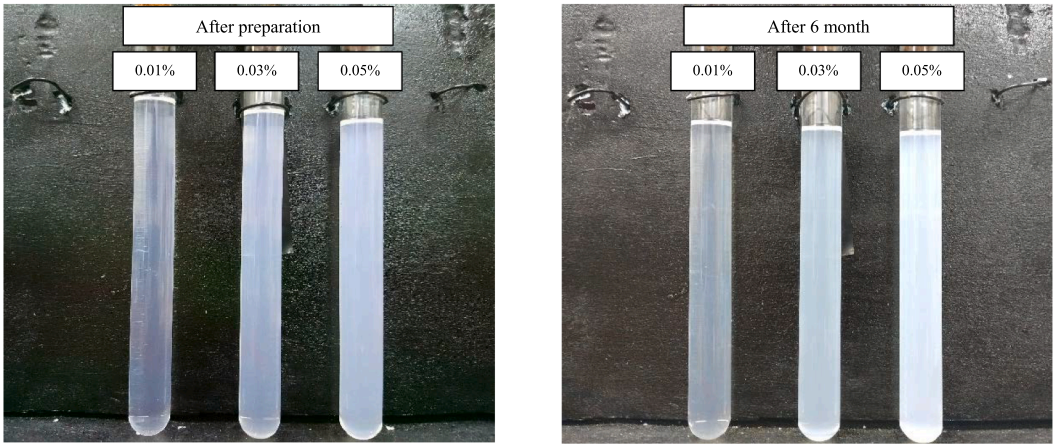

(b) Visual sedimentation for Al_2O_3/PAG nanolubricants

Fig. 4. The visual sedimentation observation of nanolubricants.

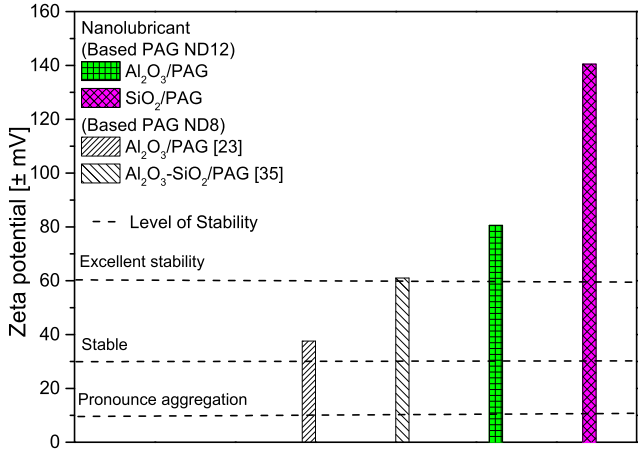

Fig. 5. Stability of the nanolubricants according to zeta potential measurements.

parameters such as superheating, subcooling, and refrigerant mass flow rate. The understanding of these parameters is crucial to fully understanding the characteristics of the AAC-R1234yf system with the use of Al_2O_3/PAG and SiO_2/PAG nanolubricants. Fig. 6 shows the analysis of the relationship between superheating and the initial refrigerant charge for various compressor speeds. The superheating decreased with an increase in the initial refrigerant charge. The AAC system in the present work maintained the same refrigerant temperature before the compressor inlet regardless of refrigerant charge and compressor speed. The saturation temperature was low at the lower initial refrigerant charge because of low pressure at the low-pressure side of the AAC system. Thus, the difference in the superheat was high at a low initial refrigerant charge as presented in Fig. 6. According to Fig. 6(a), almost all of the superheat for the AAC system with SiO_2/PAG nanolubricants was comparable and lower at some points when compared to the AAC-PAG system (except at the 900 rpm compressor speed). Lower superheating indicated that the AAC-SiO_2/PAG system absorbs more heat at the evaporator. Superheating of the AAC-SiO_2/PAG system with 0.03% volume concentration decreased at all initial refrigerant charges and compressor speeds. This was due to the properties of nanolubricants in the AAC system with better thermal properties [37,38]. However, as shown in Fig. 6(b), the AAC system with Al_2O_3/PAG nanolubricants achieved higher superheating than the AAC-PAG system. Thus, less heat was absorbed by the refrigerant vapour in the multi-channel evaporator tube. Furthermore, Fig. 6(b) shows that superheating is greater in the AAC-Al_2O_3/PAG system than in the AAC-SiO_2/PAG system. In this experiment, the low-pressure side of the AAC system with SiO_2/PAG and Al_2O_3/PAG nanolubricants was observed to be lower than that of the AAC system with PAG lubricant. This condition reduced the

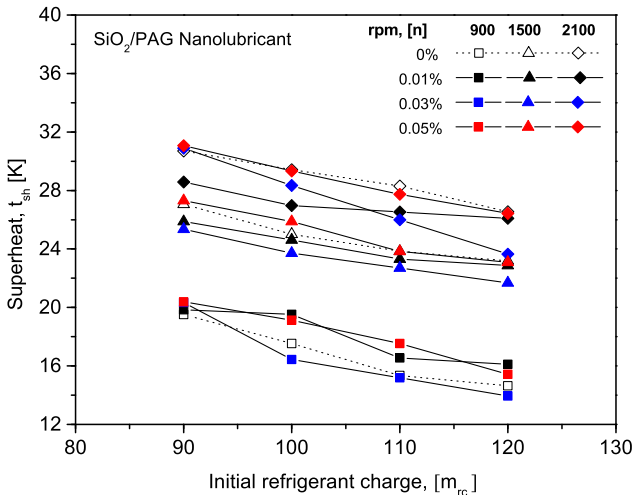

a) SiO_2/PAG nanolubricants

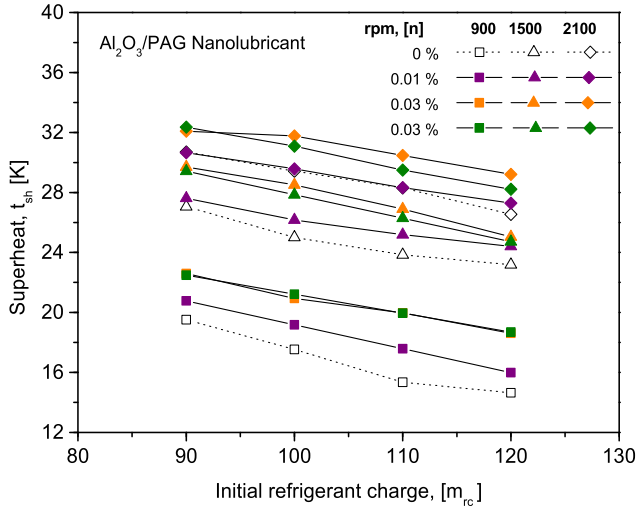

b) Al_2O_3/PAG nanolubricants

Fig. 6. Comparison of superheat for different initial refrigerant charges of nanolubricants.

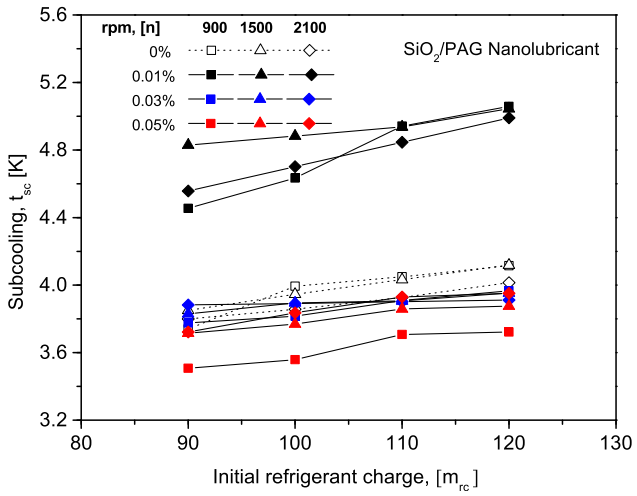

a) SiO_2/PAG nanolubricants

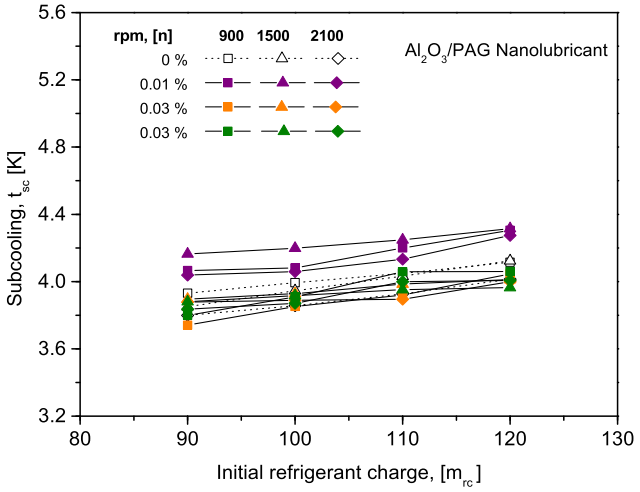

b) Al_2O_3/PAG nanolubricants

Fig. 7. Comparison of subcooling for different initial refrigerant charges of nanolubricants.

superheating value of the AAC system with nanolubricants due to the low saturation temperature. However, the Al_2O_3/PAG-AAC system performed with higher superheating value than the SiO_2/PAG-AAC system due to the Al_2O_3/PAG nanolubricant exhibiting a higher viscosity than the SiO_2/PAG nanolubricant [32]. Higher viscosity was usually associated with the pressure drop of the refrigeration system [39].

Fig. 7 shows the subcooling of the AAC system for various initial refrigerant charges and different compressor speeds. The subcooling tended to increase with the speed of the compressor. This was due to the refrigerant mass flow rate, which increases with the compressor speed increment. Subcooling also increased with the increase in the initial refrigerant charge. The trends were similar for all working conditions and were applicable for different types of nanolubricants. Overall, the subcooling of the nanolubricants is comparable to PAG (within ± 10%). However, the results showed a minor reduction at some points in volume concentrations. Previous research also found the same finding of insignificant increment in subcooling with the use of nanoparticles [40]. However, the subcooling for AAC-SiO_2/PAG and AAC-Al_2O_3/PAG systems performed better for 0.01% volume concentration, with higher subcooling than the base PAG lubricants. Therefore, subcooling was not a factor in the increment of cooling capacity for the AAC-SiO_2/PAG system and compressor work reduction in the AAC-Al_2O_3/PAG system. As shown in Fig. 7(a) and (b), the subcooling trend was stronger at a low volume concentration of 0.01% for both nanolubricants. At a low volume concentration of 0.01% nanolubricants, the pressure of the AAC system was increased at the high-pressure side. Thus, increasing the saturation temperature at the high-pressure side of the AAC system. This probably occurred when the TXV becomes restricted by the presence of nanoparticles in the system. However, this condition was not applicable for nanolubricants at a higher volume concentration than 0.01% because of the improvement in heat transfer properties [32]. The AAC system with nanolubricants at 0.03% and 0.05% volume concentrations were demonstrated to have lower subcooling than the base PAG lubricants. At this point, the AAC system operated with a better effect of pressure reduction, thus reducing refrigerant saturation before the TXV inlet.

The experimental data of the refrigerant mass flow rate for AAC systems with Al_2O_3/PAG and SiO_2/PAG nanolubricants are shown in Fig. 8(a) and 8(b), respectively, by varying the initial refrigerant charges for compressor speed ranging from 900 to 2100 rpm. The refrigerant mass flow rate in Fig. 8 was increased with an increment of the initial refrigerant charge and compressor speed. The mass flow rate of SiO_2/PAG nanolubricants was greater than that of PAG lubricants, as shown in Fig. 8(a). This was due to the low superheating value for SiO_2/PAG

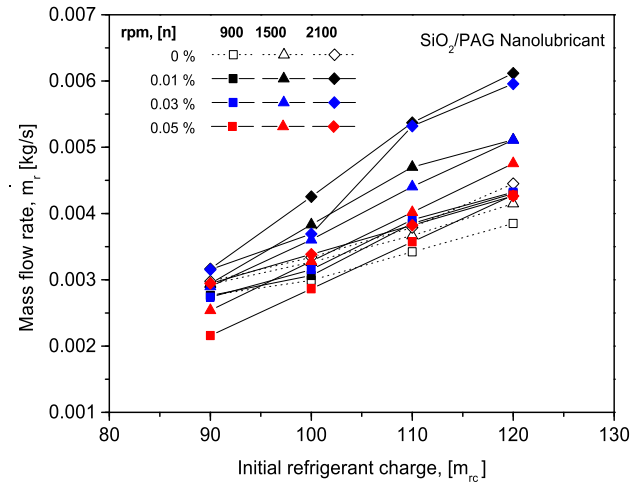

a) SiO_2/PAG nanolubricants

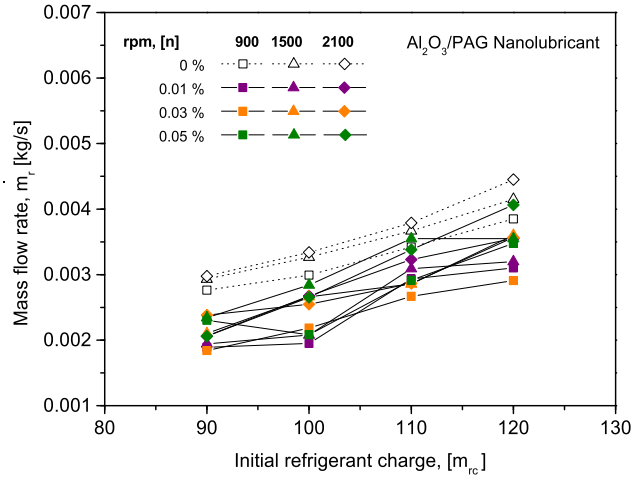

b) Al_2O_3/PAG nanolubricants

Fig. 8. Mass flow rate comparison for different initial refrigerant charge of nanolubricants.

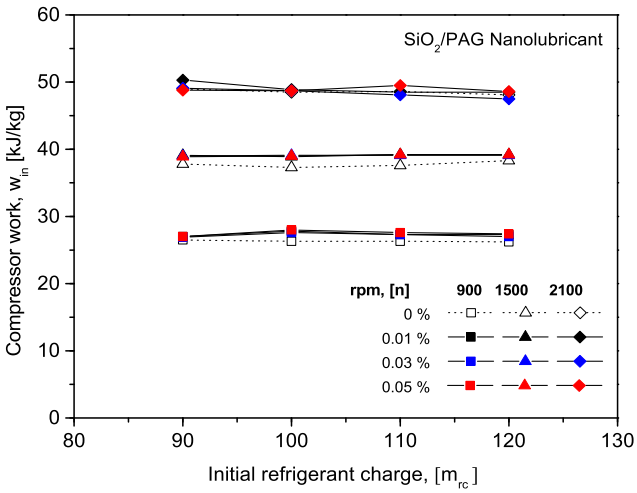

a) SiO_2/PAG nanolubricants

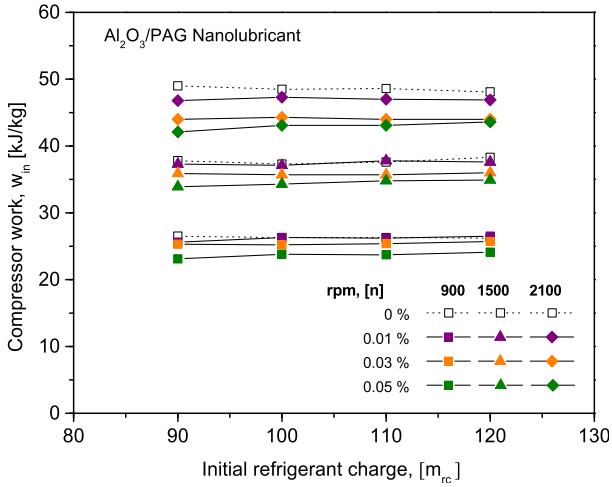

b) Al_2O_3/PAG nanolubricants

Fig. 9. Compressor work for different refrigerant charges of nanolubricants.

nanolubricants, as discussed and presented in Fig. 6(a). The present AAC system used a thermostatic expansion valve (TXV) as a throttling device. When the AAC system experienced a low superheating value, the TXV would respond by adjusting the system pressure and the refrigerant mass flow rate. As shown in Fig. 8(b), the AAC-Al_2O_3/PAG system had a lower refrigerant mass flow rate than the AAC-PAG system. This condition existed because the AAC-Al_2O_3/PAG system provided higher superheating values, as presented in Fig. 6(b). Moreover, the viscosity of Al_2O_3/PAG nanolubricant is higher than PAG lubricant, hence the possibility to increase the pressure drop during the evaporation process [39].

3.3. Compressor performance

The performance characteristics of the AAC compressor operating with PAG lubricant, Al_2O_3/PAG and SiO_2/PAG nanolubricants were presented in this section for various experimental inputs and conditions. Fig. 9 shows the work done by the AAC compressor using SiO_2/PAG and Al_2O_3/PAG nanolubricants by varying the initial refrigerant charges for compressor speeds from 900 to 2100 rpm. The compressor work increased linearly with the initial refrigerant charge and the speed of the compressor. It seemed possible that these results were due to the compressor stroke increment with increasing compressor rotation and the amount of initial refrigerant charge [8,41]. The compressor work done for the AAC-SiO_2/PAG system was slightly higher by up to 2% compared to the AAC-PAG system, as shown in Fig. 9**(a)**, but this difference was insignificant. The AAC-SiO_2/PAG system had a low superheating rate and a high refrigerant mass flow rate, so the work done by the compressor was slightly higher than the AAC-PAG system. It was worth noting that Al_2O_3/PAG nanolubricant promoted 7.2% less compressor work than the original PAG lubricant, as shown in Fig. 9**(b)**. Overall, the AAC system with Al_2O_3/PAG nanolubricant entailed lower power input than SiO_2/PAG nanolubricant at the same operating condition. This was due to the higher thermal conductivity and better tribology characteristics of Al_2O_3/PAG nanolubricant than SiO_2/PAG nanolubricant [24,38].

The AAC power input by an AAC compressor using SiO_2/PAG and Al_2O_3/PAG nanolubricants with varying initial refrigerant charges for compressor speeds ranging from 900 to 2100 rpm is shown in Fig. 10(a) and 10(b). The compressor power input for the AAC-SiO_2/PAG system was greater than that of the AAC-PAG system and the AAC-Al_2O_3 system, as shown in Fig. 10(a). The AAC-SiO_2/PAG system had a high degree of compressor work done. Consequently, the compressor power input was also slightly higher than the other systems. Lower compressor work by the AAC system using Al_2O_3/PAG nanolubricant resulted in lower power input, which is further illustrated in Fig. 10(b). The AAC system with Al_2O_3/PAG nanolubricant promoted less compressor power input, up to 27.1% lower than the original PAG lubricant. In addition, the trend for compressor power input was also comparable with the trend of the

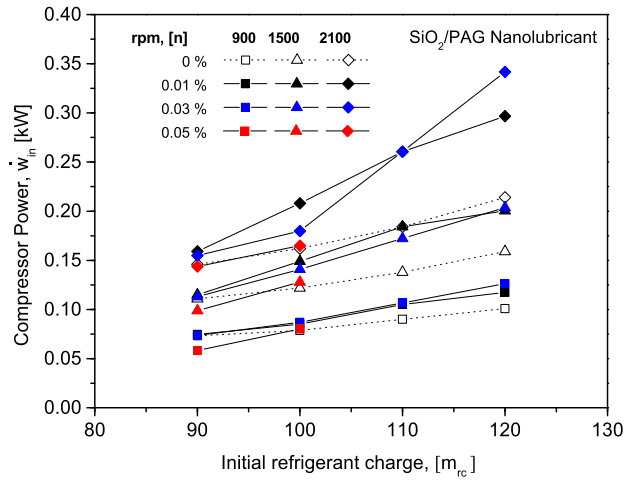

a) SiO_2/PAG nanolubricants

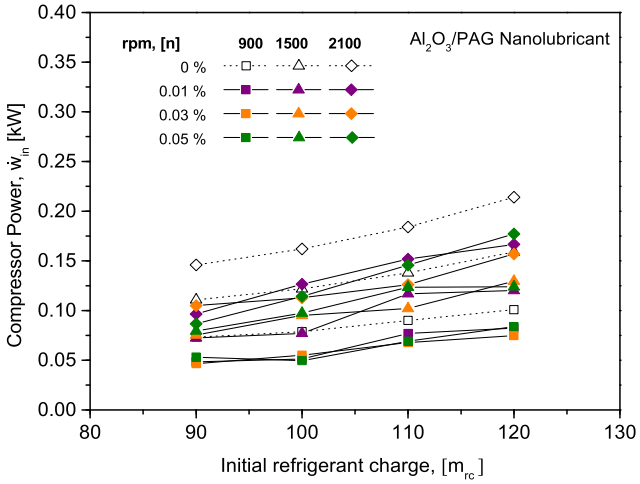

b) Al_2O_3/PAG nanolubricants

Fig. 10. Comparison of compressor power at the different refrigerant charges of nanolubricants.

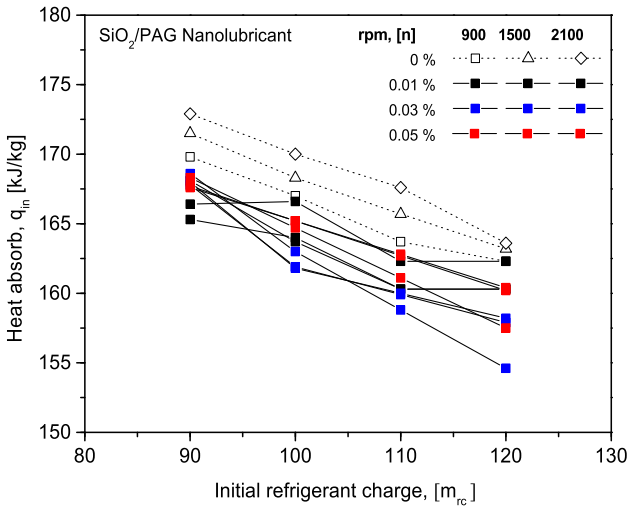

a) SiO_2/PAG nanolubricants

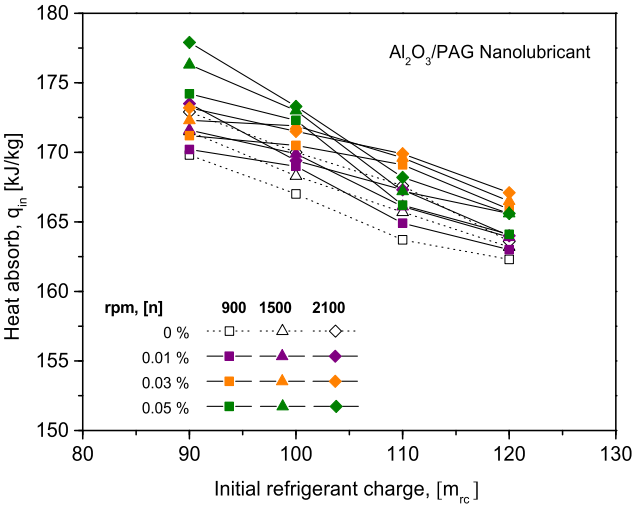

b) Al_2O_3/PAG nanolubricants

Fig. 11. Comparison of heat absorb for different refrigerant charge of nanolubricants.

previous compressor work. The AAC compressor power inputs were increased with increasing compressor speed and initial refrigerant charges. In this study, the refrigerant mass flow rate and the compressor work were found to be influenced by the increment of AAC compressor power input. This finding confirmed the association between the AAC compressor power input, work done, and the refrigeration mass flow rate, which had been observed by previous studies [23,42].

3.4. Cooling performance

The ability of the AAC evaporator to absorb heat and the cooling capacity is vital to evaluating the AAC-R1234yf cooling system. Fig. 11 (a) and (b) show the experimental data of Al_2O_3/PAG and SiO_2/PAG nanolubricants for heat absorb by the AAC evaporator at different refrigerant charges. Both graphs show the inverse relationship between heat absorption and initial refrigerant charges at various compressor speeds and are applicable for both nanolubricants. The AAC-SiO_2/PAG system in Fig. 11(a) shows lower evaporator heat absorption than the AAC-PAG and AAC-Al_2O_3/PAG systems in Fig. 11(b). However, this was considered insignificant because the decrement was only 2.6% lower than the PAG lubricants. The AAC system with high refrigerant mass flow rates may cause a reduction in the heat absorption value and vice versa. In contrast, the AAC system with Al_2O_3/PAG nanolubricants recorded 1.3% higher heat absorption than PAG lubricants, as presented in Fig. 11(b). This was probably due to the better thermal properties exhibited by Al_2O_3/PAG nanolubricants than SiO_2/PAG nanolubricants [32]. In this case, Al_2O_3/PAG nanolubricants was concluded to behave with better heat absorption than SiO_2/PAG nanolubricants.

Fig. 12(a) and (b) depict the relationship between cooling capacity and initial refrigerant charge at different compressor speeds. By looking at the graph, it can be concluded that the cooling capacity increases with an increase in the initial refrigerant charges and speeds. The results in Fig. 10(a) are somewhat revealing in several ways. Firstly, the SiO_2/PAG nanolubricants with volume concentrations of 0.01 and 0.03% performed with higher capacity heating in the AAC system for up to 15.7 and 15.1%, respectively, better than the base PAG lubricants. Secondly, the AAC-SiO_2/PAG system with 0.05% volume concentration had slightly lower cooling performance, up to 6%, than the PAG lubricants. The variation in the viscosity of nanolubricants may explain this phenomenon. The reduction of cooling capacity was observed for SiO_2/PAG nanolubricants at a volume concentration of more than 0.03%.

On the other hand, Fig. 12(b) shows the cooling capacity of the AAC system with Al_2O_3/PAG nanolubricants. The cooling capacity for Al_2O_3/PAG nanolubricants was recorded at an average of 19.9% lower compared to the AAC-PAG system. Although the AAC-Al_2O_3/PAG system had a good heat absorption performance, the low mass flow rate

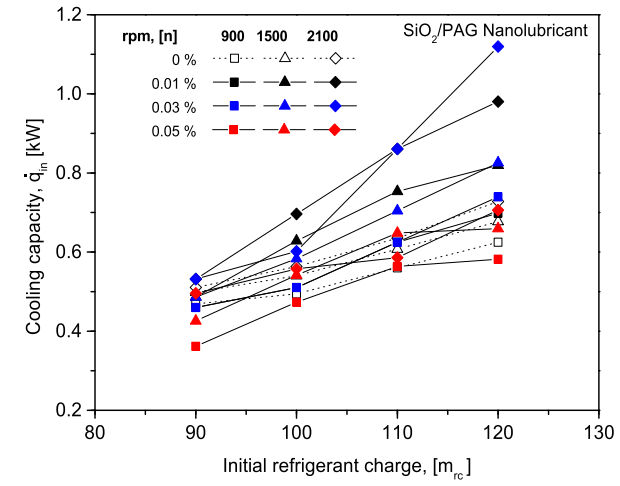

a) SiO_2/PAG nanolubricants

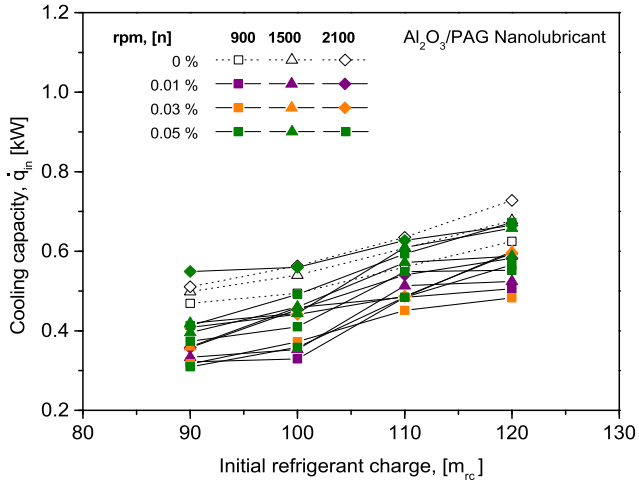

b) Al_2O_3/PAG nanolubricants

Fig. 12. Comparison of cooling capacity for the different refrigerant charges of nanolubricants.

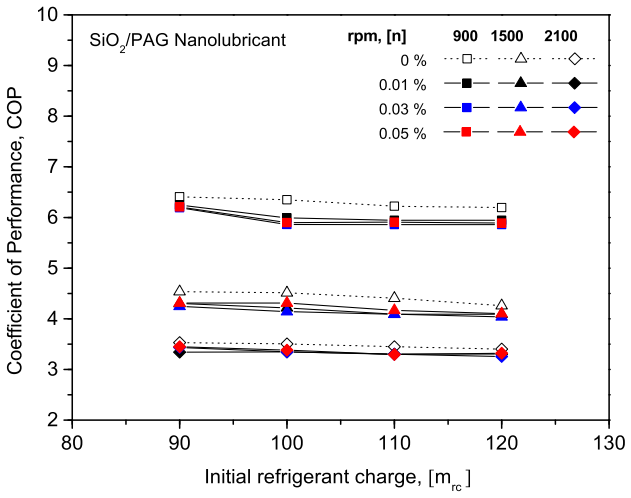

a) SiO_2/PAG nanolubricants

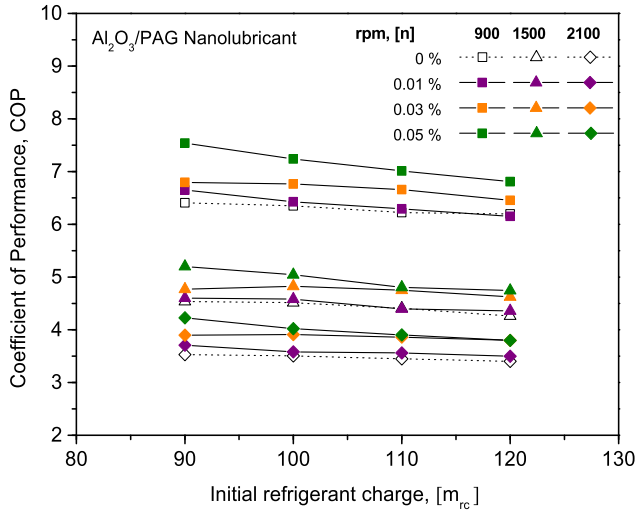

b) Al_2O_3/PAG nanolubricants

Fig. 13. Comparison of COP for nanolubricants at different refrigerant charges.

results can hinder the overall cooling performance. In a nutshell, the reason for the low cooling capacity of the AAC system with Al_2O_3/PAG nanolubricants was the high superheat rate and low refrigerant mass flow rate, as discussed in the previous section. According to a previous study, SiO_2 nanoparticles inside a vapour compression system performed better in terms of cooling capacity than Al_2O_3 nanoparticles [43]. The AAC-Al_2O_3/PAG system has higher heat absorption compared to the AAC-SiO_2/PAG system. The AAC system's high superheat is due to the starved condition at the evaporator, which is caused by a lower refrigerant mass flow rate. In this case, Al_2O_3/PAG nanolubricants have a relatively higher viscosity than SiO_2/PAG nanolubricants. This condition will increase the risk of pressure drop in the refined pipe area inside the evaporator. Hence, the Al_2O_3/PAG nanolubricant tends to have high heat absorption.

3.5. Overall system performance

Fig. 13 illustrates the variation of the ratio for the evaporator to power compressor, or coefficient of performance (COP), at different initial refrigerant charges and compressor speeds. From the graph, the COP was almost constant with increasing initial refrigerant charge. Furthermore, the COP was decreased with increasing compressor speed, as shown in Fig. 13(a) and 13(b). This was due to the variation of compressor work as discussed in Fig. 9. The compressor work was also increased by increasing the compressor speed and going beyond the enhancement of the cooling performance. The findings in Fig. 13(a) and (b) correspond to some experiments in the literature [23,42,44]. The AAC-SiO_2/PAG system recorded a lower COP with an average decrement of 4.4% compared to the AAC-PAG system. However, these decrements were counterbalanced by increasing cooling capacity, with an average increment of 12.2%. It should be noted that AAC-Al_2O_3/PAG system produced better COP than the AAC-PAG system, with an average enhancement of 9.8%. In addition, better COP performance was reported for nanolubricants at higher volume concentrations. This trend was in agreement with the previous finding, whereby the compressor work and the performance enhancement are increased with the volume concentration of nanolubricants.

The negative value in the COP enhancement analysis was observed in Fig. 14(a) for the AAC-SiO_2/PAG system. The COP reduction for the AAC-SiO_2/PAG system occurred because of high power consumption, as shown in Fig. 10. However, the drawback of COP reduction for the AAC-SiO_2/PAG system was considered insignificant due to a small decrement of less than 5% compared to the substantial improvement in cooling capacity in Fig. 12. In contrast, the COP enhancement for the AAC-Al_2O_3/PAG system in Fig. 14(b) was increased with volume concentration and was higher than the AAC-PAG and AAC-SiO_2/PAG systems as presented in Fig. 14(a). The COP increment with the volume

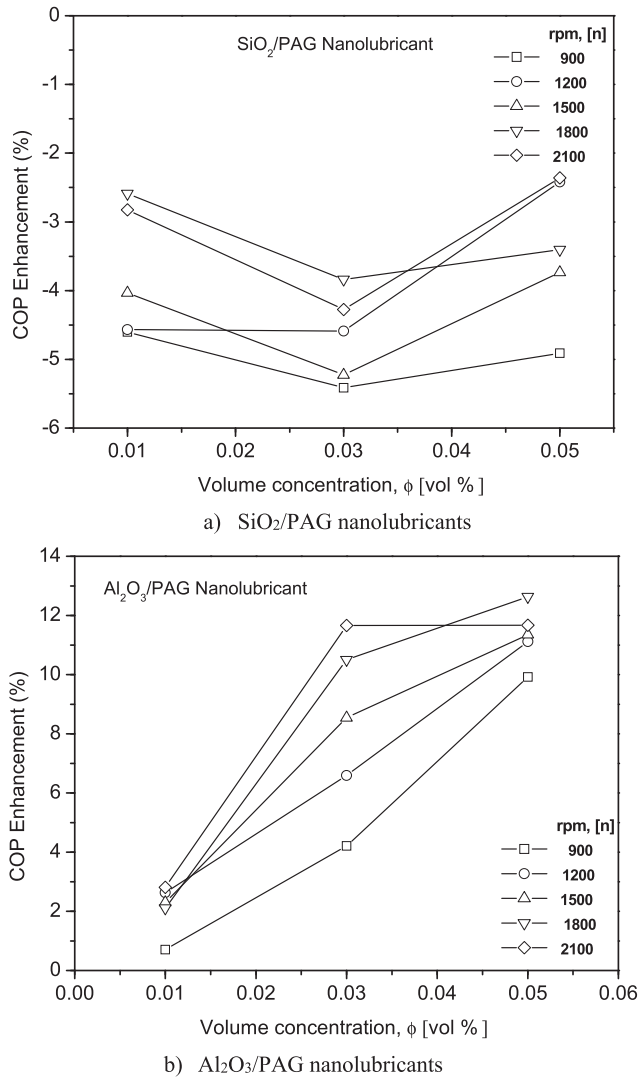

Fig. 14. Comparison of COP enhancement for nanolubricants at different refrigerant charges.

concentration was due to the reduction of the compressor work and supported by the results in Fig. 9. Similar observations were made by Redhwan et al. [23] for AAC performance with Al_2O_3/PAG nanolubricant and R134a refrigerant. They concluded that the COP enhancement of nanolubricant increased with volume concentration and the optimum COP enhancement was found at 0.01% volume concentration. The different optimum volume concentration compared to the present work is due to different types of base lubricants and different system operations.

4. Conclusions

The experimental work was carried out to emphasise the overall performance and effect of different types of nanolubricants in the AAC system operating with alternative refrigerant R1234yf. Based on the stability studies, it can be concluded that the nanolubricant had good stability with minimal agglomeration rate. The AAC-SiO_2/PAG system had better cooling capacity but consumed more energy with a lower COP. The average cooling capacity of the AAC-SiO_2/PAG system improved by 15.7% at 0.01% volume concentration. In contrast, the AAC-Al_2O_3/PAG system performed better with power consumption and COP improvement. The average COP and power consumption for the AAC-SiO_2/PAG system were enhanced by up to 9.8% and reduced by up to 27.1%, respectively, at 0.05% volume concentration. As a conclusion, the type of nanolubricant used in the AAC system exhibits different behaviours and contributes to variation improvement for various AAC parameters. Therefore, the combination of SiO_2 and Al_2O_3 nanoparticles in the composite form of nanolubricant is recommended for future work to enhance the cooling capacity and reduce compressor work. Also, the miscibility of nanolubricant with refrigerant in the AAC system is suggested for future research work. The durability aspect is importance for commercialization of the present nanolubricant in actual AAC system. Hence further investigation is required to extend the present work. In addition, it is feasible to use nanolubricants in the AAC system because of the small amount of Al_2O_3 nanoparticles, approximately 0.2 g per 100 ml of lubricants for a 0.05% volume concentration.

Declaration of Competing Interest

The authors declare that they have no known competing financial interests or personal relationships that could have appeared to influence the work reported in this paper.

Acknowledgements

The authors are grateful to the Universiti Malaysia Pahang for financial supports given under RDU1803169. The authors also thank the research team from Centre for Research in Advanced Fluid and Processes (Pusat Bendalir) and Advanced Automotive Liquids Laboratory (AALL), who provided insight and expertise that greatly assisted in the present research work.

References

[1] E.K. Nam, Understanding and modeling NOx emissions from air conditioned automobiles, SAE Technical Paper (2000–01-0858 (2000)) 1–17.
[2] L. Al-Ghussain, Global warming: review on driving forces and mitigation, Environ. Prog. Sustain. Energy 38 (2019) 13–21.
[3] J.M. Belman-Flores, A.P. Rodríguez-Muñoz, C.G. Pérez-Reguera, A. Mota-Babiloni, Experimental study of R1234yf as a drop-in replacement for R134a in a domestic refrigerator, Int. J. Refrig 81 (2017) 1–11.
[4] G.A. Longo, S. Mancin, G. Righetti, C. Zilio, R1234yf and R1234ze (E) as environmentally friendly replacements of R134a: Assessing flow boiling on an experimental basis, Int. J. Refrig 108 (2019) 336–346.
[5] M.C. Aral, M. Suhermanto, M. Hosoz, Performance evaluation of an automotive air conditioning and heat pump system using R1234yf and R134a, Science and Technology for the, Built Environment 27 (2020) 44–60.
[6] Y. Chen, Z. Yang, H. Liu, Y. Ge, R. Zhai, B. Feng, Z. Lv, W. Zhao, Experimental study on the contribution of R161 and R1234yf to the miscibility of R32 with lubricating oils, Appl. Therm. Eng. 115338 (2020).
[7] D. Sánchez, R. Cabello, R. Llopis, I. Arauzo, J. Catalán-Gil, E. Torrella, Energy performance evaluation of R1234yf, R1234ze(E), R600a, R290 and R152a as low-GWP R134a alternatives, Int. J. Refrig 74 (2017) 269–282.
[8] Z. Li, K. Liang, H. Jiang, Experimental study of R1234yf as a drop-in replacement for R134a in an oil-free refrigeration system, Appl. Therm. Eng. 153 (2019) 646–654.
[9] M.F. Sukri, M.N. Musa, M.Y. Senawi, H. Nasution, Achieving a better energy-efficient automotive air-conditioning system: a review of potential technologies and strategies for vapor compression refrigeration cycle, Energ. Effi. 8 (2015) 1201–1229.
[10] L. Yang, W. Jiang, W. Ji, O. Mahian, S. Bazri, R. Sadri, I.A. Badruddin, S. Wongwises, A review of heating/cooling processes using nanomaterials suspended in refrigerants and lubricants, Int. J. Heat Mass Transf. 153 (2020), 119611.
[11] A. Senthilkumar, A. Anderson, R. Praveen, Prospective of nanolubricants and nano refrigerants on energy saving in vapour compression refrigeration system – A review, Mater. Today:. Proc. 33 (2020) 886–889.
[12] W.K. Shafi, M.S. Charoo, An overall review on the tribological, thermal and rheological properties of nanolubricants, Tribol. Mater. Surf. Interfaces 15 (2020) 20–54.
[13] J. Zhang, A. Desideri, M.R. Kærn, T.S. Ommen, J. Wronski, F. Haglind, Flow boiling heat transfer and pressure drop characteristics of R134a, R1234yf and R1234ze in a plate heat exchanger for organic Rankine cycle units, Int. J. Heat Mass Transf. 108 (2017) 1787–1801.
[14] S.M. Hisham, K. Kadirgama, S.R. Devarajan Ramasamy, Enhancement of tribological behaviour and thermal properties of hybrid nanocellulose/copper (II) oxide nanolubricant, J. Adv. Res. Fluid Mech. Thermal Sci. 72 (2020) 47–54.
[15] M.K.A. Ali, X. Hou, M.A.A. Abdelkareem, Anti-wear properties evaluation of frictional sliding interfaces in automobile engines lubricated by copper/graphene nanolubricants, Friction 8 (2020) 905–916.

[16] S.I. Standard, SAE J2765 - Procedure for Measuring System COP [Coefficient of Performance] of a Mobile Air Conditioning System on a Test Bench, SAE Int. (2008) 1–20.
[17] M. Spatz, B. Minor, H. DuPont, HFO-1234yf: A low GWP refrigerant for MAC, in: SAE World Congress (VDA Alternative Refrigerant Winter Meeting), SAE, Detroit, Michigan, 2008.
[18] W.L. Brown, Polyalkylene glycols, CRC Handbook of Lubrication and Tribology 3 (1993) 253–267.
[19] Dow, Material Safety Data Sheet, Ucon Refrigerant Lubricant 213, (2013).
[20] K.A. Hamid, W.H. Azmi, R. Mamat, K.V. Sharma, Heat transfer performance of TiO_2–SiO_2 nanofluids in a tube with wire coil inserts, Appl. Therm. Eng. 152 (2019) 275–286.
[21] W.H. Azmi, K.A. Hamid, R. Mamat, K.V. Sharma, M.S. Mohamad, Effects of working temperature on thermo-physical properties and forced convection heat transfer of TiO_2 nanofluids in water–Ethylene glycol mixture, Appl. Therm. Eng. 106 (2016) 1190–1199.
[22] N.N.M. Zawawi, W.H. Azmi, A.A.M. Redhwan, M.Z. Sharif, Thermo-physical properties of metal oxides composite Nanolubricants, Journal of, Mech. Eng. 15 (2018) 28–38.
[23] A.A.M. Redhwan, W.H. Azmi, M.Z. Sharif, R. Mamat, M. Samykano, G. Najafi, Performance improvement in mobile air conditioning system using Al_2O_3/PAG nanolubricant, J. Therm. Anal. Calorim. 135 (2019) 1299–1310.
[24] M.Z. Sharif, W.H. Azmi, A.A.M. Redhwan, R. Mamat, T.M. Yusof, Performance analysis of SiO_2/PAG nanolubricant in automotive air conditioning system, Int. J. Refrig 75 (2017) 204–216.
[25] M.Z. Sharif, W.H. Azmi, A.A.M. Redhwan, N.N.M. Zawawi, R. Mamat, Improvement of nanofluid stability using 4-step UV-vis spectral absorbency analysis, J. Mech. Eng., SI 4 (2017) 233–247.
[26] A. Ghadimi, R. Saidur, H.S.C. Metselaar, A review of nanofluid stability properties and characterization in stationary conditions, Int. J. Heat Mass Transf. 54 (2011) 4051–4068.
[27] W.H. Azmi, K.V. Sharma, R. Mamat, G. Najafi, M.S. Mohamad, The enhancement of effective thermal conductivity and effective dynamic viscosity of nanofluids – A review, Renew. Sustain. Energy Rev. 53 (2016) 1046–1058.
[28] ASHRAE, Standard 41.9–2000 – Calorimeter Test Methods for Mass Flow Measurements of Volatile Refrigerants., (2000).
[29] I.M. Yusri, R. Mamat, G. Najafi, A. Razman, O.I. Awad, W.H. Azmi, W.F.W. Ishak, A.I.M. Shaiful, Alcohol based automotive fuels from first four alcohol family in compression and spark ignition engine: A review on engine performance and exhaust emissions, Renew. Sustain. Energy Rev. 77 (2017) 169–181.
[30] S.U. Ilyas, R. Pendyala, N. Marneni, Stability of Nanofluids, in: V.S. Korada, N. Hisham B Hamid (eds.) Engineering Applications of Nanotechnology: From Energy to Drug Delivery, Springer International Publishing, Cham, 2017, pp. 1-31.
[31] D.D. Kumar, A.V. Arasu, A comprehensive review of preparation, characterization, properties and stability of hybrid nanofluids, Renew. Sustain. Energy Rev. 81 (2018) 1669–1689.
[32] A.A.M. Redhwan, W.H. Azmi, M.Z. Sharif, R. Mamat, N.N.M. Zawawi, Comparative study of thermo-physical properties of SiO_2 and Al_2O_3 nanoparticles dispersed in PAG lubricant, Appl. Therm. Eng. 116 (2017) 823–832.
[33] N.N.M. Zawawi, W.H. Azmi, M.Z. Sharif, A.I.M. Shaiful, Composite nanolubricants in automotive air conditioning system: An investigation on its performance, IOP Conf. Ser.: Mater. Sci. Eng. 469 (2019), 012078.
[34] N.N.M. Zawawi, W.H. Azmi, A.A.M. Redhwan, M.Z. Sharif, M. Samykano, Experimental investigation on thermo-physical properties of metal oxide composite nanolubricants, Int. J. Refrig 89 (2018) 11–21.
[35] N.N.M. Zawawi, W.H. Azmi, M.Z. Sharif, G. Najafi, Experimental investigation on stability and thermo-physical properties of Al_2O_3–SiO_2/PAG nanolubricants with different nanoparticle ratios, J. Therm. Anal. Calorim. 135 (2019) 1243–1255.
[36] W. Yu, H. Xie, A review on nanofluids: preparation, stability mechanisms, and applications, J. Nanomater. 2012 (2012) 1–17.
[37] N.N.M. Zawawi, W.H. Azmi, A.A.M. Redhwan, M.Z. Sharif, Coefficient of friction and wear rate effects of different composite nanolubricant concentrations on Aluminium 2024 plate, in: IOP Conference Series: Materials Science and Engineering, Vol. 257, IOP Publishing, 2017, pp. 012065.
[38] A.R.M. Aminullah, W.H. Azmi, A.A.M. Redhwan, M.Z. Sharif, N.N.M. Zawawi, K. Kadirgama, M.N.S. Ashraf, Tribology investigation of automotive air condition (AAC) compressor by using Al_2O_3/PAG nanolubricant, J. Mech. Eng. 5 (2018) 49–61.
[39] M. Youbi-Idrissi, J. Bonjour, M.F. Terrier, C. Marvillet, F. Meunier, Oil presence in an evaporator: experimental validation of a refrigerant/oil mixture enthalpy calculation model, Int. J. Refrig 27 (2004) 215–224.
[40] S.J. Kim, T. McKrell, J. Buongiorno, L.-W. Hu, Subcooled flow boiling heat transfer of dilute alumina, zinc oxide, and diamond nanofluids at atmospheric pressure, Nucl. Eng. Des. 240 (2010) 1186–1194.
[41] F. Illán-Gómez, J.R. García-Cascales, Experimental comparison of an air-to-water refrigeration system working with R134a and R1234yf, Int. J. Refrig 97 (2019) 124–131.
[42] H. Cho, C. Ryu, Y. Kim, H.Y. Kim, Effects of refrigerant charge amount on the performance of a transcritical CO_2 heat pump, Int. J. Refrig 28 (2005) 1266–1273.
[43] O.S. Ohunakin, D.S. Adelekan, T.O. Babarinde, R.O. Leramo, F.I. Abam, C. D. Diarra, Experimental investigation of TiO_2-, SiO_2- and Al_2O_3-lubricants for a domestic refrigerator system using LPG as working fluid, Appl. Therm. Eng. 127 (2017) 1469–1477.
[44] J. Navarro-Esbrí, F. Molés, Á. Barragán-Cervera, Experimental analysis of the internal heat exchanger influence on a vapour compression system performance working with R1234yf as a drop-in replacement for R134a, Appl. Therm. Eng. 59 (2013) 153–161.
[45] S. Aldrich, Safety Data Sheet, Aluminium Oxide (2013).
[46] I. Zakaria, W.H. Azmi, W.A.N.W. Mohamed, R. Mamat, G. Najafi, Experimental investigation of thermal conductivity and electrical conductivity of Al_2O_3 nanofluid in water-ethylene glycol mixture for proton exchange membrane fuel cell application, Int. Commun. Heat Mass Transfer 61 (2015) 61–68.